inorganics

MDPI

Article

Effects of Introducing Methoxy Groups into the Ancillary Ligands in Bis(diimine) Copper(I) Dyes for Dye-Sensitized Solar Cells

Annika Büttner, Sven Y. Brauchli, Edwin C. Constable and Catherine E. Housecroft *

Department of Chemistry, University of Basel, Building 1096, Mattenstrasse 24a, CH-4058 Basel, Switzerland; annika.buettner@unibas.ch (A.B.); sven.brauchli@bluewin.ch (S.Y.B.); edwin.constable@unibas.ch (E.C.C.)

* Correspondence: catherine.housecroft@unibas.ch

Received: 23 March 2018; Accepted: 6 April 2018; Published: 10 April 2018

Abstract: A systematic investigation of four heteroleptic bis(diimine) copper(I) dyes in n-type Dye-Sensitized Solar Cells (DSSCs) is presented. The dyes are assembled using a stepwise, on-surface assembly. The dyes contain a phosphonic acid-functionalized 2,2′-bipyridine (bpy) anchoring domain (**5**) and ancillary bpy ligands that bear peripheral phenyl (**1**), 4-methoxyphenyl (**2**), 3,5-dimethoxyphenyl (**3**), or 3,4,5-trimethoxyphenyl (**4**) substituents. In masked DSSCs, the best overall photoconversion efficiency was obtained with the dye [Cu(**5**)(**4**)]$^+$ (1.96% versus 5.79% for N719). Values of J_{SC} for both [Cu(**5**)(**2**)]$^+$ (in which the 4-MeO group is electron releasing) and [Cu(**5**)(**4**)]$^+$ (which combines electron-releasing and electron-withdrawing effects of the 4- and 3,5-substituents) and are enhanced with respect to [Cu(**5**)(**1**)]$^+$. DSSCs with [Cu(**5**)(**3**)]$^+$ show the lowest J_{SC}. Solid-state absorption spectra and external quantum efficiency spectra reveal that [Cu(**5**)(**4**)]$^+$ benefits from an extended spectral range at higher energies. Values of V_{OC} are in the order [Cu(**5**)(**4**)]$^+$ > [Cu(**5**)(**1**)]$^+$ > [Cu(**5**)(**2**)]$^+$ > [Cu(**5**)(**3**)]$^+$. Density functional theory calculations suggest that methoxyphenyl character in MOs within the HOMO manifold in [Cu(**5**)(**2**)]$^+$ and [Cu(**5**)(**4**)]$^+$ may contribute to the enhanced performances of these dyes with respect to [Cu(**5**)(**1**)]$^+$.

Keywords: copper; 2,2′-bipyridine; dye-sensitized solar cell; solar energy conversion; methoxy-substitution

1. Introduction

Dye-sensitized solar cells (DSSCs) [1] convert solar to electrical energy using an optically transparent, wide-band gap semiconductor functionalized with a surface-bound dye which extends the absorption range into the visible spectrum [2–4]. The semiconductor is commonly mesoporous TiO_2 and the sensitizer is typically a ruthenium(II) complex such as the standard reference dye N719 (Scheme 1) or an organic dye in DSSCs based on n-type semiconductors. Photoconversion efficiencies (η) of up to 11–14% have been recorded using ruthenium-based, organic, or zinc(II) porphyrin-based sensitizers [5–10]. However, the scarcity of ruthenium in the Earth's crust and its associated high cost have motivated us and others to investigate the use of inorganic dyes containing Earth abundant metals. Copper(I) [11–13] and iron(II) [14,15] complexes are of primary interest. For copper-sensitized DSSCs, reported values of η in the range 3–5% [16–18] confirm the potential of DSSCs containing copper(I) dyes. When comparing these lower photoconversion efficiencies with the values obtained for state-of-the-art ruthenium(II) dyes, it is important to recognize that the dye structures and dye/electrolyte combinations in the ruthenium-based systems have been optimized for over a quarter of a century. In contrast, copper-based DSSCs are still in their infancy and, with systematic tuning of dye and electrolyte components [16,19–22] and the use of co-sensitization [18], enhanced performances are gradually being achieved.

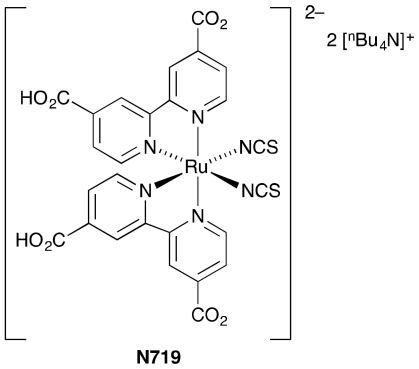

N719

Scheme 1. Structure of the ruthenium dye N719.

Most copper(I) sensitizers are bis(diimine) copper(I) complexes and "push–pull" dyes which facilitate electron injection necessarily require the use of heteroleptic complexes. To overcome the problems of rapid ligand redistribution in solution (Equation (1)), Odobel and coworkers have used the HETPHEN approach [17], in which sterically demanding groups in the 6,6′-positions of a 2,2′-bipyridine (bpy) or 2,9-positions in a 1,10-phenanthroline ligand stabilize the heteroleptic complex. Our own strategy is a "surfaces-as-ligands, surfaces as complexes" (SALSAC) approach in which the heteroleptic dye is assembled on the glass FTO/TiO_2 electrode in a stepwise manner [11]. For performance enhancement, heteroleptic dyes are essential and the SALSAC approach remains the most adaptable. It also has an advantage of allowing dye regeneration [23,24].

$$\mathbf{2}\left[\mathrm{Cu}\left(\mathrm{L^A}\right)\left(\mathrm{L^B}\right)\right]^+ \leftrightarrows \left[\mathrm{Cu}\left(\mathrm{L^A}\right)_2\right]^+ + \left[\mathrm{Cu}\left(\mathrm{L^B}\right)_2\right]^+ \quad (1)$$

For the anchoring domain in a dye in DSSCs, carboxylic acid (or carboxylate) anchors are commonly employed [25]. However, for heteroleptic copper(I) dyes, we have found that phosphonic acids are superior to carboxylic acids [11]. This is consistent with the strong binding of phosphonic acids and phosphonates to TiO_2 [26] and the applications of phosphonic acid anchors in some ruthenium dyes [27].

We have investigated the use of ancillary ligands with hole-transporting dendrons [28], but such ligands are synthetically time-intensive, and we have generally found that dyes containing structurally simple ancillary ligands [16,18,29] perform as well, if not better, than those with more elaborate architecture. In accordance with the maxim "small is beautiful" [30], we now present an investigation of the effects on DSSC performance of introducing peripheral methoxy substituents into the ancillary ligand in bis(diimine) copper(I) dyes. The ancillary ligands **1**–**4** and anchoring ligand **5** (Scheme 2) each contain methyl substituents in the 6,6′-positions of the bpy unit to stabilize the copper(I) complexes. Copper(I) prefers a tetrahedral coordination geometry, and substituents close to the copper(I) centre prevent flattening to the square-planar geometry favoured by copper(II) [31]. The ancillary ligands **1**, **2**, **3**, and **4** contain peripheral phenyl, 4-methoxyphenyl, 3,5-dimethoxyphenyl, and 3,4,5-trimethoxyphenyl substituents, respectively. We were interested to know how the overall electron-releasing behaviour of the *para*-OMe or electron-withdrawing nature of the *meta*-OMe substituents [32–34] would influence the DSSC performances of the dyes [Cu(**5**)($L_{ancillary}$)]$^+$ ($L_{ancillary}$ = **1**, **2**, **3**, or **4**). Such substituent effects have been used by Wu et al. to tune properties of hole-transporting materials for perovskite solar cells [35].

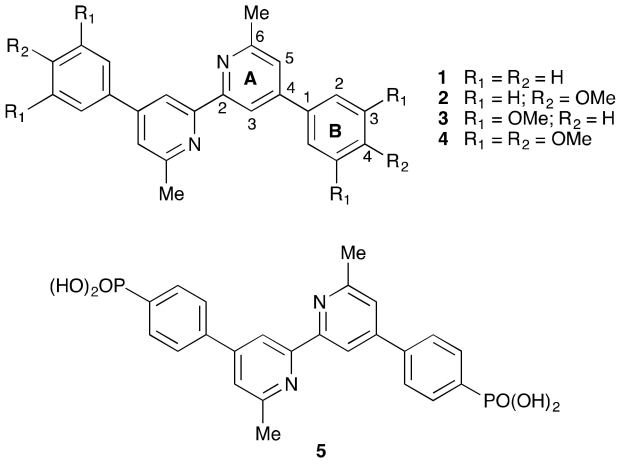

Scheme 2. Structures of ligands and atom labelling for NMR assignments.

2. Results and Discussion

2.1. Synthesis and Compound Characterization

Compounds **1**–**3** and **5** were prepared as previously reported [36–39]. Ligand **4** was synthesized using Kröhnke [40] methodology as shown in Scheme 3. The ^{1}H and ^{13}C NMR spectra of **4** are displayed in Figures S1 and S2 and were assigned by COSY, NOESY, HMQC, and HMBC methods. A cross peak in the NOESY spectrum between H^{Me} and H^{A5} distinguished the signals for H^{A3} and H^{A5}. The methyl groups of the methoxy substituents give rise to ^{1}H NMR resonances at δ 3.97 and 3.92 ppm (relative integrals of 2:1) while the signal assigned to the protons of the 6,6′-dimethyl groups appears at δ 2.72 ppm.

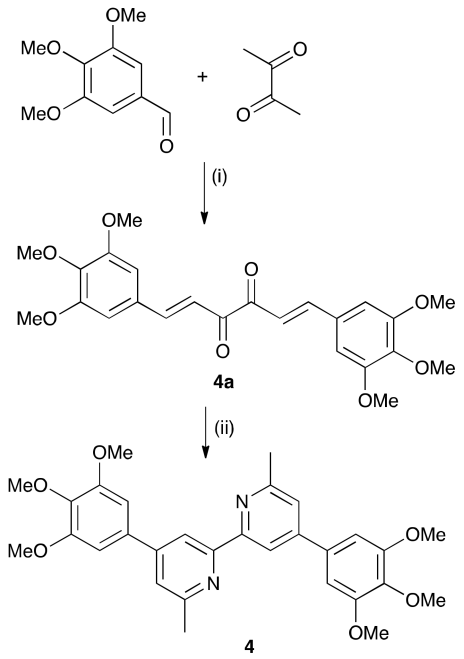

Scheme 3. Synthesis of **4**. Conditions: (i) piperidine, MeOH, reflux, overnight; (ii) NH_4OAc, EtOH, reflux, overnight. Yields: **4a** 13.0%; **4** 23.1%.

The reaction of $[Cu(MeCN)_4][PF_6]$ with ligands **1**, **2**, **3**, or **4** yielded the orange-red homoleptic complexes $[Cu(\mathbf{1})_2][PF_6]$, $[Cu(\mathbf{2})_2][PF_6]$, $[Cu(\mathbf{3})_2][PF_6]$, and $[Cu(\mathbf{4})_2][PF_6]$, respectively. We have

previously described [Cu(**2**)$_2$][PF$_6$], and the spectroscopic properties of the batch prepared in this study were fully in accord with the reported data [37]. Figures S3–S8 show ^{1}H and ^{13}C NMR spectra of [Cu(**1**)$_2$][PF$_6$], [Cu(**3**)$_2$][PF$_6$], and [Cu(**4**)$_2$][PF$_6$]. Figure 1 shows the ^{1}H NMR spectrum of [Cu(**4**)$_2$][PF$_6$] as a representative example. The spectra were assigned by 2D methods. For [Cu(**1**)$_2$][PF$_6$], the ^{13}C NMR signals for the phenyl ring C–H ^{13}C nuclei appear in the range δ 130.9 to 128.4 ppm. On comparing [Cu(**1**)$_2$][PF$_6$] to [Cu(**3**)$_2$][PF$_6$], the signal for C^{B3} shifts to δ 162.6 ppm, consistent with the OMe groups attached to C^{B3}. Signals for C^{B2} and C^{B4} appear at δ 106.7 and 102.2 ppm. In [Cu(**4**)$_2$][PF$_6$], nuclei C^{B3} and C^{B4} are characterized by ^{13}C NMR signals at δ 154.2 and 139.9 ppm, respectively. In [Cu(**4**)$_2$][PF$_6$], the ^{13}C NMR resonances for C^{A2} and C^{A6} could not be resolved in the 1D spectrum (Figure S8), and the HMBC spectrum was used to locate them at δ 157.4 and 152.1 ppm (Figure 2). In the respective electrospray mass spectrums of [Cu(**1**)$_2$][PF$_6$], [Cu(**3**)$_2$][PF$_6$], and [Cu(**4**)$_2$][PF$_6$], the base peak corresponded to the [M–PF$_6$]$^+$ ion at major isotopomer (m/z) = 735.24, 975.31, and 1095.30, respectively. Each peak envelope showed the predicted isotope pattern (Figure S9).

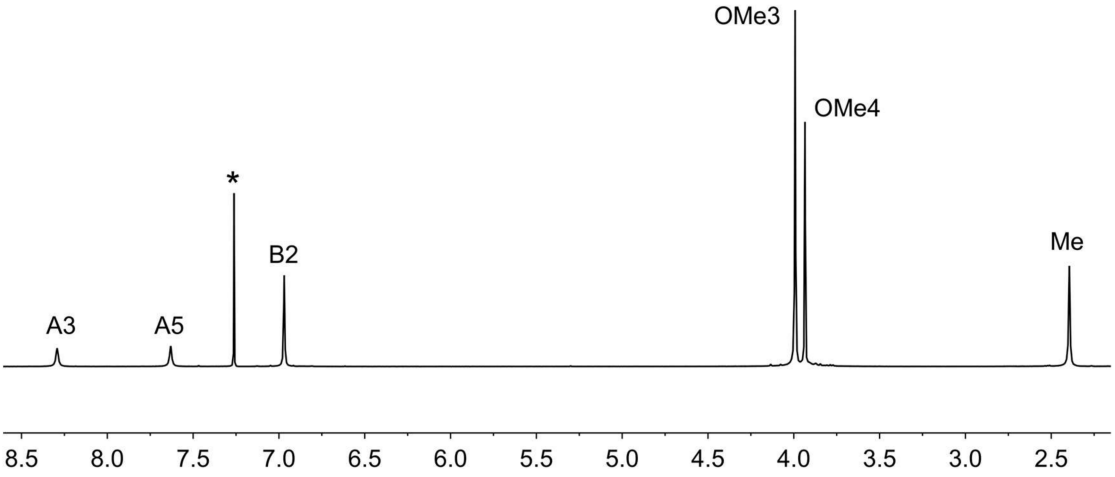

Figure 1. The 500 MHz ^{1}H NMR spectrum of [Cu(**4**)$_2$][PF$_6$] ($CDCl_3$). * = residual $CHCl_3$. Chemical shifts in δ/ppm. See Scheme 1 for labelling.

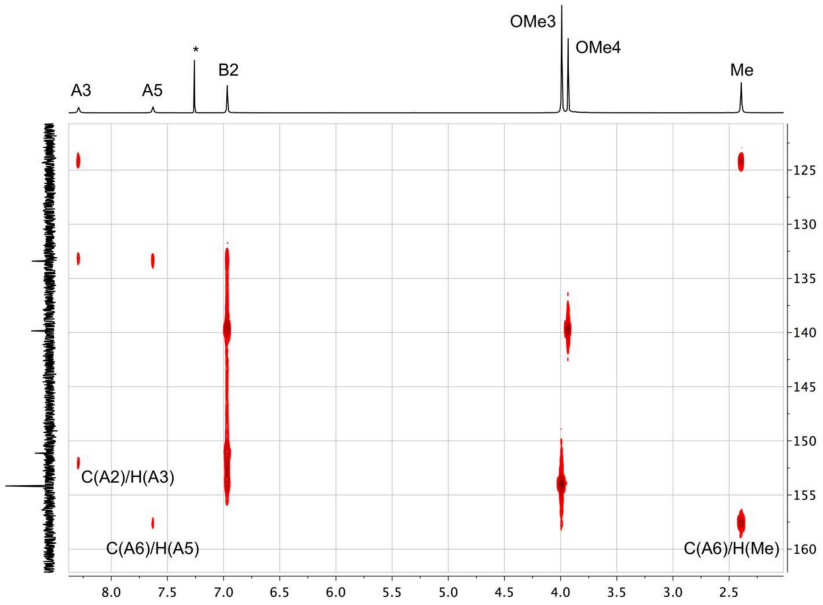

Figure 2. Part of the HMBC spectrum (500 HMz ^{1}H, 126 MHz ^{13}C) of [Cu(**4**)$_2$][PF$_6$] ($CDCl_3$). * = residual $CHCl_3$.

2.2. Solution and Solid-State Absorption Spectra

The solution absorption spectra of the homoleptic complexes are presented in Figure 3 and the absorption maxima and intensity data are given in Table 1. We include the spectrum of [Cu(**2**)$_2$][PF$_6$] for comparison. The previously reported data was for an MeCN solution [37] whereas, here, the data is for CH_2Cl_2 solutions. Intense absorption bands below 390 nm arise from $\pi^*\leftarrow\pi$ transitions in [Cu(**1**)$_2$][PF$_6$] and from $\pi^*\leftarrow\pi$ and $\pi^*\leftarrow n$ transitions in the compounds containing methoxy groups. Each compound exhibits a metal-to-ligand charge transfer (MLCT) band in the range 482–486 nm.

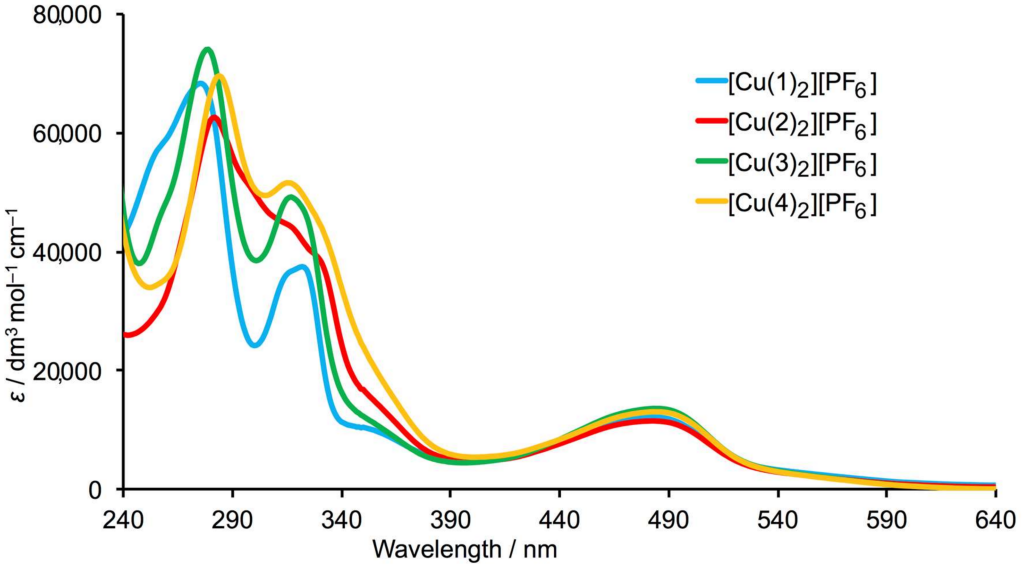

Figure 3. Solution absorption spectra of the homoleptic copper(I) complexes (CH_2Cl_2, 1×10^{-5} mol dm^{-3}).

Table 1. Absorption maxima for homoleptic copper(I) complexes (CH_2Cl_2, 5×10^{-5} mol dm^{-3}) [a].

Complex	λ_{max}/nm (ε_{max}/dm^3 mol^{-1} cm^{-1})	
	$\pi^*\leftarrow\pi$ and $\pi^*\leftarrow n$	MLCT
[Cu(**1**)$_2$][PF$_6$]	255sh (56,600), 275 (68,300), 322 (37,400), 356sh (10,900)	483 (11,400)
[Cu(**2**)$_2$][PF$_6$][a]	282 (62,500), 316sh (44,300), 329sh (39,000), 357sh (14,100)	484 (11,400)
[Cu(**3**)$_2$][PF$_6$]	278 (73,900), 318 (49,000), 354sh (11,400)	486 (13,600)
[Cu(**4**)$_2$][PF$_6$]	285 (69,400), 316 (51,600)	482 (13,100)

[a] The absorption spectrum of a MeCN solution of [Cu(**2**)$_2$][PF$_6$] has previously been reported [37].

Heteroleptic dyes [Cu(**5**)(L$_{ancillary}$)]$^+$ were assembled on transparent TiO_2 electrodes (i.e., no TiO_2 scattering layer) by sequential dipping of the glass FTO/TiO_2 electrodes in baths containing anchoring ligand **5** in DMSO (Scheme 2) and one of the homoleptic complexes in CH_2Cl_2 (Figure 4a). This process leads to the assembly of the surface-anchored heteroleptic dye, exemplified in Figure 4b by [Cu(**5**)(**1**)]$^+$. The solid-state absorption spectra of the functionalized electrodes are shown in Figure 5, with the MLCT band appearing at 475 nm for [Cu(**5**)(**1**)]$^+$ and [Cu(**5**)(**2**)]$^+$, 476 nm for [Cu(**5**)(**3**)]$^+$, and 473 nm for [Cu(**5**)(**4**)]$^+$. A blue-shift of ca.10 nm is observed on going from the solution spectrum of [Cu(L$_{ancillary}$)$_2$]$^+$ to the solid-state spectrum of the surface-bound [Cu(L$_{anchor}$)(L$_{ancillary}$)]$^+$ complex. The protonation state of the phosphonic acid is not known.

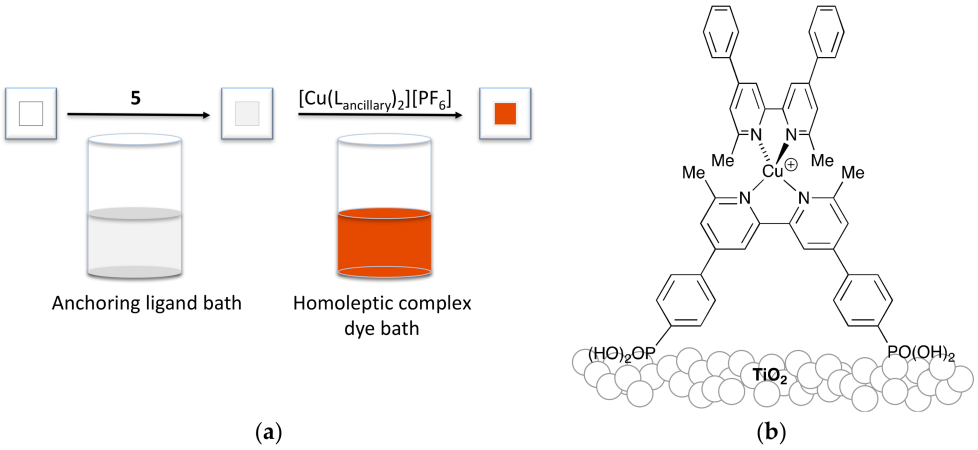

Figure 4. (**a**) The SALSAC approach to functionalization of a glass FTO/TiO_2 electrode surface with a heteroleptic [Cu(L_{anchor})($L_{ancillary}$)]$^+$ dye. Transparent electrodes were used for absorption spectroscopy, and TiO_2 with a scattering layer was used for DSSC measurements. (**b**) Surface-anchored [Cu(**5**)(**1**)]$^+$.

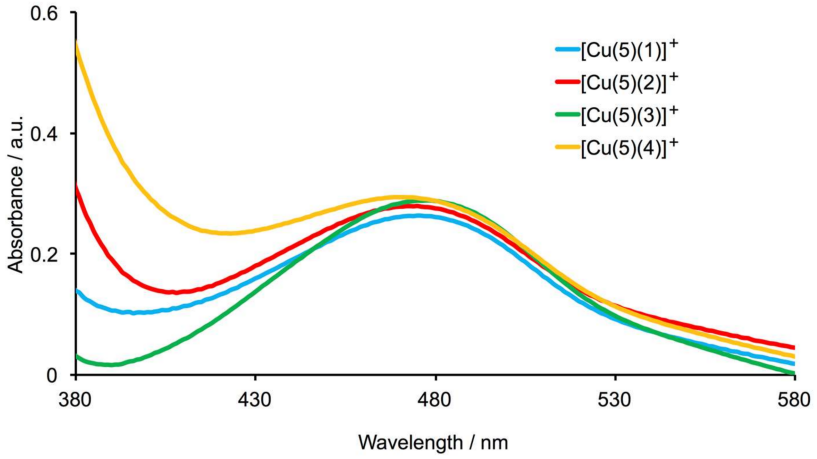

Figure 5. Solid-state absorption spectra of FTO/TiO_2 electrodes functionalized with [Cu(**5**)($L_{ancillary}$)]$^+$ dyes ($L_{ancillary}$ = **1**, **2**, **3**, or **4**).

2.3. DSSC Performances

Working electrodes with a scattering layer were functionalized with the heteroleptic dyes [Cu(**5**)($L_{ancillary}$)]$^+$ dyes ($L_{ancillary}$ = **1**, **2**, **3**, or **4**) as summarized in Figure 4, and duplicate masked DSSCs for each dye were assembled (see Materials and Methods). Reference DSSCs containing N719 (Scheme 1) were also fabricated (see Materials and Methods), and the plots of current density (J) against potential (V) in Figure 6 confirm the reproducibility of their performances. We have observed [16] that copper-dye functionalized DSSCs may improve in performance after initial fabrication. The J–V measurements for the DSSCs were, therefore, made on the day of sealing the cells (day 0) and repeated seven days later. The performance parameters for these masked DSSCs are given in Table 2. DSSCs with [Cu(**5**)(**1**)]$^+$ and [Cu(**5**)(**3**)]$^+$ were referenced to N719 cell 1, with [Cu(**5**)(**2**)]$^+$ to N719 cell 2, and with [Cu(**5**)(**4**)]$^+$ to N719 cell 3 (Table 2). The final column in Table 2 gives relative values of the efficiency η with respect to N719 set at 100%, and (on the day that the DSSCs were made) values range from 24.2% and 25.4% for [Cu(**5**)(**3**)]$^+$ to 30.2% and 33.9% for [Cu(**5**)(**4**)]$^+$. Comparisons of the DSSC parameters for days 0 and 7 indicate that the devices are stable over this period but that there are no ripening effects [41,42] leading to significantly enhanced performance.

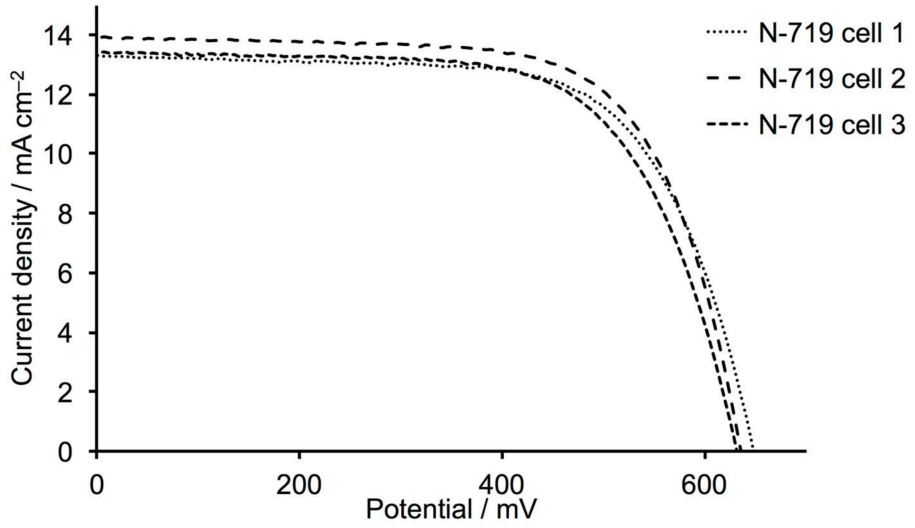

Figure 6. *J–V* curves for three N719 reference cells (DSSCs were fully masked).

Table 2. Performance parameters (under 1 sun illumination) of duplicate, masked DSSCs (mask aperture calibrated and ca. 0.06 cm^2) with $[Cu(\mathbf{5})(L_{ancillary})]^+$ ($L_{ancillary}$ = **1**, **2**, **3,** or **4**) on the day of sealing the cells, and after seven days. The data is compared to a DSSC containing N719 and relative η values are with respect to N719 set at 100% [a].

Dye	On the Day of DSSC Fabrication				
	J_{SC}/mA cm^{-2}	V_{OC}/mV	*ff*/%	η/%	Relative η/%
$[Cu(\mathbf{5})(\mathbf{1})]^+$	4.27	545	71	1.66	28.7
$[Cu(\mathbf{5})(\mathbf{1})]^+$	4.20	536	70	1.58	27.3
N719 (cell 1) [a]	13.29	647	67	5.79	100
$[Cu(\mathbf{5})(\mathbf{2})]^+$	4.87	528	71	1.82	30.1
$[Cu(\mathbf{5})(\mathbf{2})]^+$	4.74	524	72	1.80	29.8
N719 (cell 2) [a]	13.91	635	68	6.04	100
$[Cu(\mathbf{5})(\mathbf{3})]^+$	3.68	528	73	1.43	25.4
$[Cu(\mathbf{5})(\mathbf{3})]^+$	3.90	516	72	1.46	24.2
N719 (cell 3) [a]	13.42	631	66	5.62	100
$[Cu(\mathbf{5})(\mathbf{4})]^+$	4.79	567	72	1.96	33.9
$[Cu(\mathbf{5})(\mathbf{4})]^+$	4.68	550	68	1.75	30.2
N719 (cell 1) [a]	13.29	647	67	5.79	100
Dye	**7 Days after DSSC Fabrication**				
	J_{SC}/mA cm^{-2}	V_{OC}/mV	*ff*/%	η/%	Relative η/%
$[Cu(\mathbf{5})(\mathbf{1})]^+$	4.22	580	70	1.72	29.7
$[Cu(\mathbf{5})(\mathbf{1})]^+$	4.19	573	70	1.68	29.0
N719 (cell 1) [a]	12.70	670	68	5.80	100
$[Cu(\mathbf{5})(\mathbf{2})]^+$	4.33	569	71	1.74	28.0
$[Cu(\mathbf{5})(\mathbf{2})]^+$	5.02	565	65	1.86	30.0
N719 (cell 2) [a]	13.23	690	68	6.21	100
$[Cu(\mathbf{5})(\mathbf{3})]^+$	3.23	541	74	1.29	21.8
$[Cu(\mathbf{5})(\mathbf{3})]^+$	4.30	562	70	1.70	28.8
N719 (cell 1) [a]	13.05	673	67	5.91	100
$[Cu(\mathbf{5})(\mathbf{4})]^+$	4.75	580	67	1.86	32.1
$[Cu(\mathbf{5})(\mathbf{4})]^+$	4.64	593	65	1.80	31.0
N719 (cell 3) [a]	12.70	670	68	5.80	100

[a] Three different N719 reference cells were used: cell 1 for measurements with $[Cu(\mathbf{5})(\mathbf{1})]^+$ and $[Cu(\mathbf{5})(\mathbf{3})]^+$, cell 2 for measurements with $[Cu(\mathbf{5})(\mathbf{3})]^+$, and cell 3 for measurements with $[Cu(\mathbf{5})(\mathbf{4})]^+$.

Table 2 and the *J*–*V* curves in Figure 7 reveal that the highest short-circuit current densities (J_{SC}) are obtained for the dyes [Cu(**5**)(**2**)]$^+$ and [Cu(**5**)(**4**)]$^+$ with the 4-MeO and 3,4,5-$(MeO)_3$ substitution patterns in each phenyl ring (Scheme 2). While differences in J_{SC} are small for these two dyes, values of the open-circuit voltages (V_{OC}) are larger for [Cu(**5**)(**4**)]$^+$ than [Cu(**5**)(**2**)]$^+$. The replacement of the phenyl substituents in [Cu(**5**)(**1**)]$^+$ by 4-methoxyphenyl or 3,4,5-trimethoxyphenyl groups in [Cu(**5**)(**2**)]$^+$ and [Cu(**5**)(**4**)]$^+$, respectively, enhances J_{SC} but leads to a fall in V_{OC} for [Cu(**5**)(**2**)]$^+$, as opposed to a gain in V_{OC} for [Cu(**5**)(**4**)]$^+$. While Figure 7 shows this for the best performing cells, the scatter plots in Figure 8 confirm that the trend is true for the duplicate cells. The presence of the 4-MeO group is critical. The dye [Cu(**5**)(**3**)]$^+$ containing 3,5-dimethoxyphenyl groups exhibits the lowest values of V_{OC} and J_{SC} of all four dyes (Figures 7 and 8). The trends are consistent with the competitive mesomeric (+M) and inductive (−I) effects of the methoxy substituents. Electrons are released by the +M effect but are withdrawn by the −I effect. On going from **1** to **2**, the electron-releasing 4-methoxy groups [32–34] enhance the "push–pull" characteristics of the dye, resulting in higher J_{SC}. In contrast, introducing the electron-withdrawing 3,5-dimethoxy substituents [32–34] upon replacing ancillary ligand **1** by **3** has a detrimental effect on DSSC performance. Ancillary ligand **4** combines the effects of both ligands **2** and **3** and, interestingly, this results in the best-performing dye. DSSCs with [Cu(**5**)(**4**)]$^+$ exhibit both the highest V_{OC} and J_{SC} (Figures 7 and 8) and photoconversion efficiences up to 33.9% relative to N719 set at 100%. The trends in J_{SC} are reflected in the external quantum efficiency (EQE) spectra displayed in Figure 9. Table 3 gives values of EQE_{max} and λ_{max}, and values of λ_{max} are similar to the absorption maxima in the solid-state spectra in Figure 5. The slightly lower EQE_{max} for [Cu(**5**)(**4**)]$^+$ versus [Cu(**5**)(**2**)]$^+$ is offset by the broader spectral range extending to higher energies; this is also observed in the solid-state absorption spectrum (Figure 5).

Table 3. EQE maxima for duplicate DSSCs containing dyes [Cu(**5**)($L_{ancillary}$)]$^+$ ($L_{ancillary}$ = **1**–**4**).

Dye	λ_{max}/nm	EQE_{max}/%
[Cu(**5**)(**1**)]$^+$	470	42.7
[Cu(**5**)(**1**)]$^+$	470	41.9
[Cu(**5**)(**2**)]$^+$	480	46.5
[Cu(**5**)(**2**)]$^+$	480	45.3
[Cu(**5**)(**3**)]$^+$	470	39.1
[Cu(**5**)(**3**)]$^+$	470	38.0
[Cu(**5**)(**4**)]$^+$	470	45.3
[Cu(**5**)(**4**)]$^+$	470	44.9

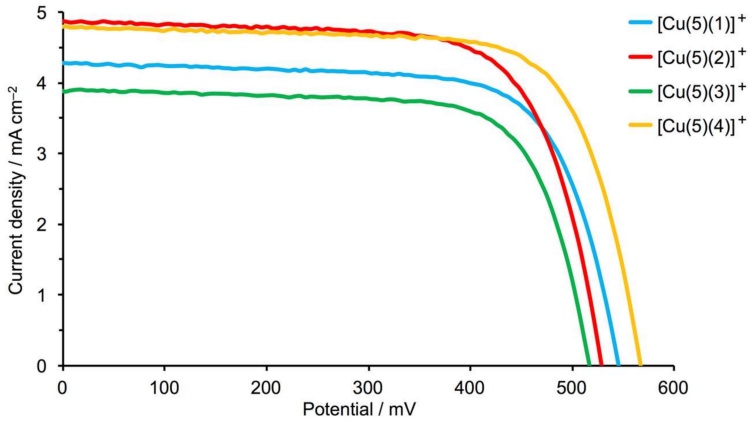

Figure 7. *J*–*V* curves for the best performing DSSCs containing dyes [Cu(**5**)($L_{ancillary}$)]$^+$ ($L_{ancillary}$ = **1**–**4**).

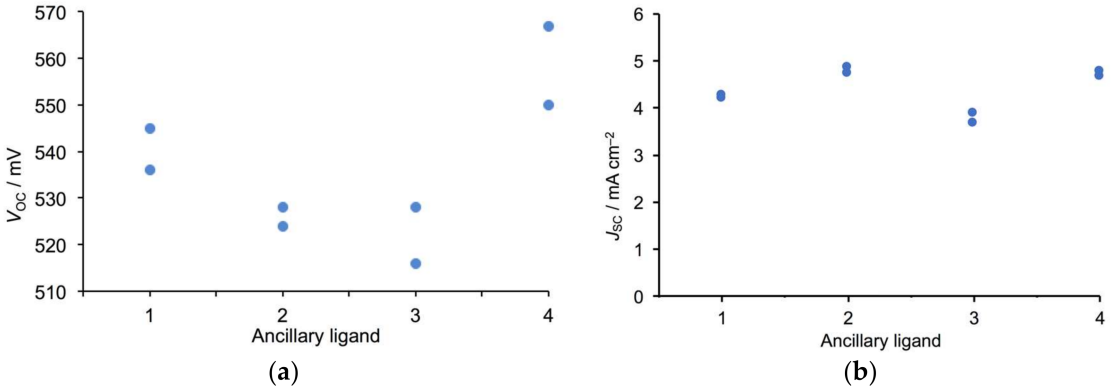

Figure 8. Trends in values of (**a**) V_{OC} and (**b**) J_{SC} for duplicate DSSCs containing the dyes [Cu(**5**)(**1**)]$^+$ (Ph groups), [Cu(**5**)(**2**)]$^+$ (4-MeOC_6H_4 groups), [Cu(**5**)(**3**)]$^+$ (3,5-$(MeO)_2C_6H_3$ groups), or [Cu(**5**)(**4**)]$^+$ (3,4,5-$(MeO)_3C_6H_2$ groups).

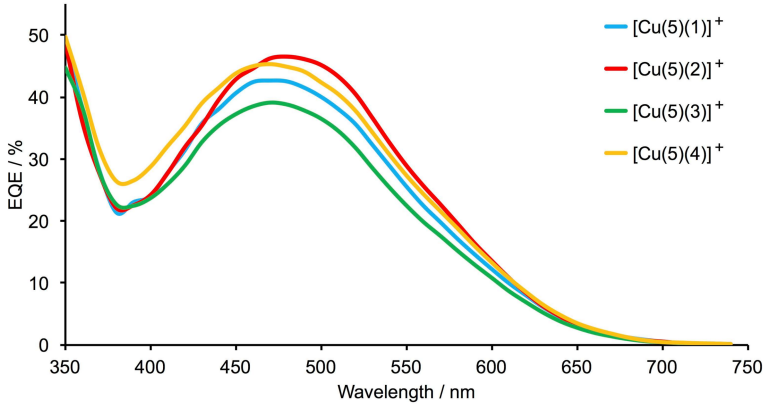

Figure 9. EQE spectra for the best performing DSSCs containing dyes [Cu(**5**)($L_{ancillary}$)]$^+$ ($L_{ancillary}$ = **1**–**4**).

2.4. Characteristics of the HOMO and LUMO Manifolds

Ground state density functional theory (DFT) calculations were used to examine how methoxy-substitution affects the characteristics of the molecular orbitals in the HOMO and LUMO manifolds of the dyes. In an earlier study of bis(diimine) copper(I) complexes, we demonstrated that use of different atomic orbital basis sets (6-311++G** basis set on all atoms, 6-311++G** on Cu, 6-31G* on C, H and N, or 6-31G* on all atoms) strongly influences the calculated absorption spectra but had no significant effect upon the characteristics of the MOs lying in the HOMO and LUMO manifolds [43]. In the present investigation, we therefore employed a 6-31G* basis set on all atoms to reduce the computational burden, and we focus mainly on orbital composition.

The characters of the MOs from HOMO−3 to LUMO+1 and energy levels are shown in Figures 10 and 11. For all sensitizers, the LUMO is localized on the anchoring ligand while the LUMO+1 is localized on the bpy unit of the ancillary ligand. The energy gap between the LUMO and LUMO+1 is similar in each complex (Figure 11). Inspection of the character of the HOMO in each complex is instructive. The HOMO is essentially centered on copper. Although, in each of the methoxy-functionalized dyes there are additional contributions from the ancillary ligand extending over the peripheral aryl groups. This is most apparent for [Cu(**5**)(**2**)]$^+$. The appearance of dominant methoxyphenyl character in HOMO−3 in [Cu(**5**)(**2**)]$^+$ and [Cu(**5**)(**4**)]$^+$, as well in HOMO−2 and HOMO−3 in [Cu(**5**)(**3**)]$^+$, may aid hole transport over the ancillary ligand. This is reminiscent of [Cu(**5**)(**7**)]$^+$ (**7** = 4,4′-bis(4-iodophenyl)-6,6-dimethyl-2,2′-bipyridine), for which we have suggested that

the improved performance of DSSCs containing [Cu(**5**)(**7**)]$^+$ with respect to other halo-analogues may be associated with better electron transfer from the electrolyte over the 4-IC_6H_4 substituent [16].

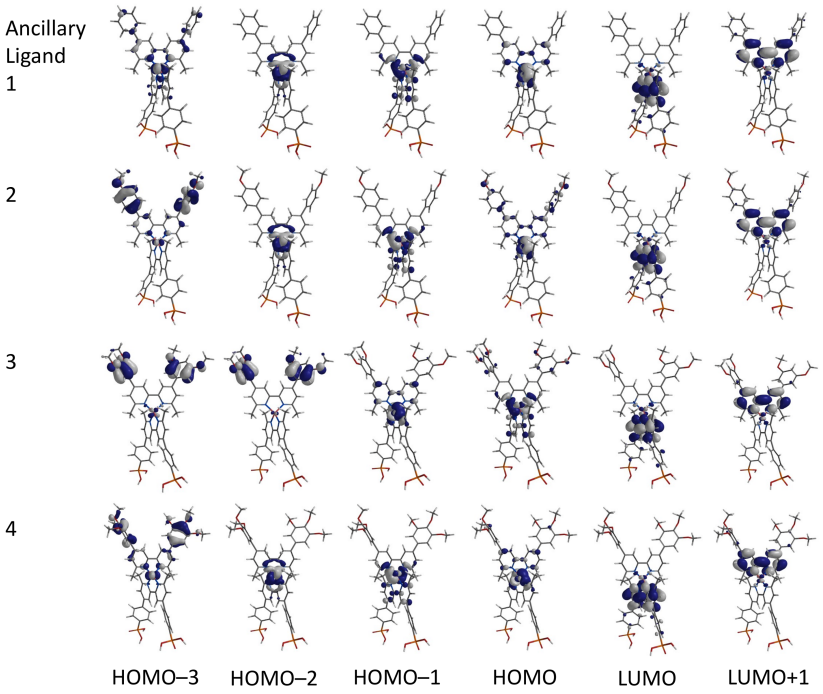

Figure 10. Characteristics of the MOs from HOMO−3 to LUMO+1 of [Cu(**5**)(**1**)]$^+$ (top row), [Cu(**5**)(**2**)]$^+$, [Cu(**5**)(**3**)]$^+$, and [Cu(**5**)(**4**)]$^+$ (bottom row). The orientation of the complex is the same in each figure, with anchor **5** as the lower ligand. (DFT B3LYP level with a 6-31G* basis set in vacuum.).

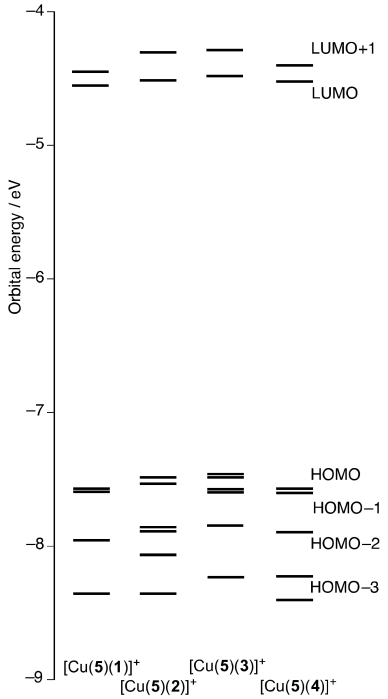

Figure 11. Orbital energies carried at DFT B3LYP level with a 6-31G* basis set in vacuum for [Cu(**5**)(**1**)]$^+$, [Cu(**5**)(**2**)]$^+$, [Cu(**5**)(**3**)]$^+$, and [Cu(**5**)(**4**)]$^+$.

3. Materials and Methods

3.1. General

^{1}H and ^{13}C NMR spectra were recorded on a Bruker Avance III-500 NMR spectrometer (Bruker BioSpin AG, Fällanden, Switzerland), and ^{1}H and ^{13}C chemical shifts were referenced to residual solvent peaks with respect to δ(TMS) = 0 ppm. Solution and solid-state absorption spectra were recorded on a Cary 5000 spectrophotometer, (Agilent Technologies Inc., Santa Clara, CA, United States), respectively. Electrospray ionization (ESI) mass spectra were recorded on a Shimadzu LCMS-2020 instrument (Shimadzu Schweiz GmbH, Roemerstr, Switzerland), and high resolution ESI mass spectra were recorded on a Bruker maXis 4G QTOF instrument (Bruker Daltonics GmbH, Faellanden, Switzerland).

Compounds **1**–**3** and **5** were prepared as previously reported and spectroscopic data matching those reported [36–39] [Cu(MeCN)$_4$][PF$_6$] were prepared by the method in the literature [44], and [Cu(**2**)$_2$][PF$_6$] has previously been reported [37]. 3,4,5-Trimethoxybenzaldehyde was purchased from Sigma-Aldrich (Buchs, Switzerland).

3.2. Compound **4a**

A suspension of 3,4,5-trimethoxybenzaldehyde (18.0 g, 89.9 mmol) and piperidine (0.897 mL, 8.99 mmol) in MeOH (150 mL) was heated to 50 °C and stirred until all solids had dissolved. A solution of 2,3-butanedione (3.97 mL, 45.0 mmol) in MeOH (30 mL) was added dropwise. The reaction mixture was heated to reflux for 4 h and slowly cooled to room temperature over 1 h. The precipitate that formed was separated by filtration and washed with Et$_2$O. Compound **4a** was isolated as an orange solid (3.65 g, 11.3 mmol, 13.0%). ^{1}H NMR (500 MHz, CDCl$_3$) δ/ppm 7.81 (d, J = 16.1 Hz, 2H, H^{alkene}), 7.42 (d, J = 16.1 Hz, 2H, H^{alkene}), 6.89 (s, 4H, H^{B2}), 3.92 (s, 18 H, H^{OMe}).

3.3. Compound **4**

Compound **4a** (858 mg, 1.94 mmol), 1-(2-oxopropyl)pyridinium chloride (666 mg, 3.88 mmol), and NH$_4$OAc (4.49 g, 58.2 mmol) were dissolved in EtOH (100 mL) and heated to reflux overnight (~15 h). The solution was cooled to room temperature, and the precipitate that formed was separated by filtration and washed with Et$_2$O. Ligand **4** was isolated as an orange solid (230 mg, 0.445 mmol, 23.1%). ^{1}H NMR (500MHz, CDCl$_3$) δ/ppm 8.40 (d, J = 1.7 Hz, 2H, H^{A3}), 7.35 (d, J = 1.6 Hz, 2H, H^{A5}), 6.93 (s, 4H, H^{B2}), 3.97 (s, 12H, H^{OMe3}), 3.92 (s, 6H, H^{OMe4}), 2.72 (s, 6H, H^{Me}). ^{13}C NMR (126 MHz, CDCl$_3$) δ/ppm 158.6 (C^{A6}), 156.7 (C^{A2}), 153.8 (C^{B3}), 150.0 (C^{A4}), 139.0 (C^{B4}), 134.9 (C^{B1}), 121.4 (C^{A5}), 116.9 (C^{A3}), 104.8 (C^{B2}), 61.2 (C^{OMe3}), 56.8 (C^{OMe4}), 24.9 (C^{Me}). ESI MS m/z 517.22 (calc. 517.23).

*3.4. [Cu(**1**)$_2$][PF$_6$]*

Ligand **1** (90.2 mg, 0.268 mmol) and [Cu(NCMe)$_4$][PF$_6$] (49.9 mg, 0.134 mmol) were dissolved in MeCN (25 mL) and stirred overnight at room temperature. The reaction mixture was then filtered, the solvent was removed under reduced pressure, and the resulting dark red solid was washed several times with Et$_2$O to yield [Cu(**1**)$_2$][PF$_6$] as dark red solid (95 mg, 0.108 mmol, 80.4%). ^{1}H NMR (500 MHz, CD$_3$CN) δ/ppm 8.68 (s, 4H, H^{A3}), 7.96 (d, J = 7.1 Hz, 8H, H^{B2}), 7.85 (s, 4H, H^{A5}), 7.60 (m, 12H, H^{B3+B4}), 2.42 (s, 12H, H^{Me}). ^{13}C NMR (126 MHz, CD$_3$CN) δ/ppm 158.8 (C^{A6}), 153.3 (C^{A2}), 151.2 (C^{A4}), 138.1 (C^{B1}), 130.9 (C^{B4}), 130.3 (C^{B3}), 128.4 (C^{B2}), 124.6 (C^{A5}), 118.8 (C^{A3}), 25.5 (C^{Me}). ESI MS m/z 735.24 [M − PF$_6$]$^+$ (calc. 735.25). HR ESI MS m/z 735.2542 [M − PF$_6$]$^+$ (calc. 735.2543).

*3.5. [Cu(**3**)$_2$][PF$_6$]*

[Cu(**3**)$_2$][PF$_6$] was prepared in the same manner as [Cu(**1**)$_2$][PF$_6$], starting with **3** (150 mg, 0.329 mmol) and [Cu(NCMe)$_4$][PF$_6$] (61.3 mg, 0.165 mmol) in MeCN (25 mL). [Cu(**3**)$_2$][PF$_6$] was isolated as a dark red solid (135 mg, 0.121 mmol, 73.2%). ^{1}H NMR (500MHz, CD$_3$CN) δ/ppm 8.68

(s, 4H, H^{A3}), 7.83 (s, 4H, H^{A5}), 7.08 (d, J = 2.0 Hz, 8H, H^{B2}), 6.67 (s, 4H, H^{B4}), 3.89 (s, 24H, H^{OMe}), 2.34 (s, 12H, H^{Me}). ^{13}C NMR (126 MHz, CD_3CN) δ/ppm 162.6 (C^{B3}), 158.6 (C^{A6}), 153.3 (C^{A2}), 151.0 (C^{A4}), 140.2 (C^{B1}), 124.9 (C^{A5}), 119.0 (C^{A3}), 106.7 (C^{B2}), 102.2 (C^{B4}), 56.4 (C^{OMe}), 25.4 (C^{Me}). ESI MS m/z 975.31 $[M - PF_6]^+$ (calc. 975.34). HR ESI MS m/z 975.3399 $[M - PF_6]^+$ (calc. 975.3389).

*3.6. [Cu(**4**)$_2$][PF$_6$]*

Ligand **4** (226 mg, 0.437 mmol) and $[Cu(NCMe)_4][PF_6]$ (81.5 mg, 0.219 mmol) were dissolved in EtOH (25 mL) and the mixture was stirred for 4 h at room temperature. Water was added and the organic solvent removed under reduced pressure. The residue was filtered over Celite, washed with water and Et_2O, and re-dissolved in MeCN. The solvent was removed under reduced pressure yielding $[Cu(\mathbf{4})_2][PF_6]$ as a dark red solid (189 mg, 0.152 mmol, 69.5%). ^{1}H NMR (500MHz, $CDCl_3$) δ/ppm 8.29 (s, 4H, H^{A3}), 7.63 (s, 4H, H^{A5}), 6.97 (s, 8H, H^{B2+B6}), 3.99 (s, 24H, H^{OMe3}), 3.93 (s, 12H, H^{OMe4}), 2.39 (s, 12H, H^{Me}). ^{13}C NMR (126 MHz, $CDCl_3$) δ/ppm 157.4 (C^{A6}), 154.2 (C^{B3}), 152.1 (C^{A2}), 151.1 (C^{A4}), 139.9 (C^{B4}), 133.4 (C^{B1}), 124.3 (C^{A5}), 117.7 (C^{A3}), 105.0 (C^{B2}), 61.2 (C^{OMe4}), 56.7 (C^{OMe3}), 25.5 (C^{Me}). ESI MS m/z 1095.30 $[M - PF_6]^+$ (calc. 1095.38).

3.7. DSSC Fabrication

TiO_2 electrodes (Solaronix Test Cell Titania Electrodes, Solaronix SA, Aubonne, Switzerland) were washed with milliQ water and HPLC grade EtOH, heated at 450 °C for 30 min, then cooled to ca. 80 °C. The thicknesses of the transparent and scattering layers were ~9 and 3 μm, respectively, by SEM [45]. The electrodes were then placed in a DMSO solution of **5** (1.0 mM) for 24 h at room temperature. The electrodes were removed from the solution, washed with DMSO and EtOH, and dried in an N_2 stream. Each electrode was then immersed in a CH_2Cl_2 solution of $[Cu(\mathbf{1})_2][PF_6]$, $[Cu(\mathbf{2})_2][PF_6]$, $[Cu(\mathbf{3})_2][PF_6]$, or $[Cu(\mathbf{4})_2][PF_6]$ (0.1 mM) for 3 days at room temperature. After removal from the dye-bath, the electrodes were washed with CH_2Cl_2 and dried in an N_2 stream. For N719 (Solaronix SA, Aubonne, Switzerland), TiO_2 electrodes were soaked in a solution of N719 (EtOH, 0.3 mM) for 3 days. The electrodes were taken out of the dye-bath, washed with EtOH, and dried in an N_2 stream. Commercial counter electrodes (Solaronix Test Cell Platinum Electrodes, Solaronix SA, Aubonne, Switzerland) were washed with EtOH and then heated at 450 °C for 30 min to remove volatile organics.

Thermoplast hot-melt sealing foil (Solaronix Test Cell Gaskets, 60 μm, Aubonne, Switzerland) was used to join the working and counter-electrodes. The space between the electrodes was filled with electrolyte (LiI (0.1 M), I_2 (0.05 M), 1-methylbenzimidazole (0.5 M), 1-butyl-3-methylimidazolinium iodide (0.6 M) in 3-methoxypropionitrile) by vacuum backfilling through a hole in the counter electrode. Then, this hole was sealed (Solaronix Test Cell Sealings and Solaronix Test Cell Caps, Aubonne, Switzerland).

3.8. Electrodes for Solid-State Absorption Spectroscopy

Dye-functionalized electrodes were assembled using the immersion procedure above but using Solaronix Test Cell Titania Electrodes Transparent (Solaronix SA, Aubonne, Switzerland).

3.9. DSSC and External Quantum Efficiency (EQE) Measurements

The DSSCs were masked. The mask was made from a black-coloured copper sheet with an aperture (ca. 0.06 cm^2, each mask accurately calibrated) smaller than the surface area of TiO_2. Black tape was used to complete the top and side masking of each DSSC. Performance measurements were made by irradiating the DSSC from behind with a LOT Quantum Design LS0811 instrument (LOT-QuantumDesign GmbH, Darmstadt, Germany, 100 mW cm^{-2} = 1 sun, AM1.5 G conditions) and the simulated light power was calibrated with a silicon reference cell.

EQE measurements were made using a Spe Quest quantum efficiency setup (Rera Systems, Nijmegen, The Netherlands) operating with a 100 W halogen lamp (QTH) and a lambda 300 grating

monochromator (L.O.T.-Oriel GmbH & Co. KG, Darmstadt, Germany). The monochromatic light was modulated to 3 Hz using a chopper wheel (ThorLabs Inc., Newton, NJ, USA), and the cell response was amplified with a large dynamic range IV converter (Melles Griot B.V., Didam, The Netherlands) and measured with a SR830 DSP Lock-In amplifier (Stanford Research Systems Inc., Sunnyvale, CA, USA).

3.10. DFT Calculations

Ground state density functional theory (DFT) calculations were carried out using Spartan 16 (v. 2.0.9) [46] at the B3LYP level with a 6-31G* basis set in vacuum. Initial energy optimization was carried out at a semi-empirical (PM3) level.

4. Conclusions

We have prepared and characterized the homoleptic copper(I) complexes $[Cu(\mathbf{1})_2][PF_6]$, $[Cu(\mathbf{3})_2][PF_6]$, and $[Cu(\mathbf{4})_2][PF_6]$. These and $[Cu(\mathbf{2})_2][PF_6]$ have been used to assemble heteroleptic dyes on FTO/TiO_2 electrodes utilizing the SALSAC approach with the bis(phosphonic acid) **5** as the anchoring ligand. In masked n-type DSSCs, the highest efficiency η was obtained for $[Cu(\mathbf{5})(\mathbf{4})]^+$ (1.96% versus 5.79% for N719, or a relative efficiency of 33.9% with respect to N719). Although values of J_{SC} are similar for DSSCs with $[Cu(\mathbf{5})(\mathbf{2})]^+$ (electron releasing 4-MeO group in **2**) and $[Cu(\mathbf{5})(\mathbf{4})]^+$ (competitive electron-releasing and electron-withdrawing effects of 4-MeO and 3,5-$(MeO)_2$ groups in **4**), DSSCs with $[Cu(\mathbf{5})(\mathbf{2})]^+$ exhibit a lower V_{OC} than those with $[Cu(\mathbf{5})(\mathbf{4})]^+$. DSSCs with $[Cu(\mathbf{5})(\mathbf{3})]^+$ show the lowest J_{SC} and V_{OC}. Solid-state absorption spectra and EQE spectra demonstrate that $[Cu(\mathbf{5})(\mathbf{4})]^+$ benefits from an extended spectral response at higher energies. Inspection of orbital characteristics from ground state DFT calculations demonstrates that orbital character in MOs within the HOMO manifold extends to the methoxyphenyl groups in $[Cu(\mathbf{5})(\mathbf{2})]^+$ and $[Cu(\mathbf{5})(\mathbf{4})]^+$, and we propose that this may contribute to the enhanced performances of these dyes with respect to $[Cu(\mathbf{5})(\mathbf{1})]^+$.

Supplementary Materials: The following are available online at http://www.mdpi.com/2304-6740/6/2/40/s1, Figures S1–S8: NMR spectra of ligand **4** and complexes $[Cu(\mathbf{1})_2][PF_6]$, $[Cu(\mathbf{3})_2][PF_6]$ and $[Cu(\mathbf{4})_2][PF_6]$. Figure S9: ESI mass spectrum of $[Cu(\mathbf{4})_2][PF_6]$.

Acknowledgments: We thank the Swiss National Science Foundation (Grant number 200020_162631) and the University of Basel for support. We thank Maximilian Klein (University of Basel) for preparing ligand **2**, and Frederik J. Malzner (University of Basel) is acknowledged for assisting with Figure 4.

Author Contributions: Annika Büttner: Synthesis, compound characterization and DSSC measurements; Sven Y. Brauchli: synthesis and contributions to NMR spectroscopic data; Edwin C. Constable: project concepts and manuscript writing; Catherine E. Housecroft: project concepts and manuscript writing.

Conflicts of Interest: The authors declare no conflicts of interest.

References

1. O'Reagan, B.; Grätzel, M. A low-cost, high-efficiency solar cell based on dye-sensitized colloidal TiO_2 films. *Nature* **1991**, *353*, 737–740. [CrossRef]
2. Nazeeruddin, M.K.; Baranoff, E.; Grätzel, M. Dye-sensitized solar cells. A brief overview. *Sol. Energy* **2011**, *85*, 1172–1178. [CrossRef]
3. Grätzel, M. Recent Advances in Sensitized Mesoscopic Solar Cells. *Acc. Chem. Res.* **2009**, *42*, 1788–1798. [CrossRef] [PubMed]
4. Grätzel, M. Solar Energy Conversion by Dye-Sensitized Photovoltaic Cells. *Inorg. Chem.* **2005**, *44*, 6841–6851. [CrossRef] [PubMed]
5. Yella, A.; Lee, H.W.; Tsao, H.N.; Yi, C.; Chandiran, A.K.; Nazeeruddin, M.K.; Diau, E.W.; Yeh, C.Y.; Zakeeruddin, S.M.; Grätzel, M. Porphyrin-sensitized solar cells with cobalt (II/III)-based redox electrolyte exceed 12 percent efficiency. *Science* **2011**, *334*, 629–634. [CrossRef] [PubMed]
6. Higashino, T.; Imahori, H. Porphyrins as excellent dyes for dye-sensitized solar cells: Recent developments and insights. *Dalton Trans.* **2015**, *44*, 448–463. [CrossRef] [PubMed]

7. Xie, Y.; Tang, Y.; Wu, W.; Wang, Y.; Liu, J.; Li, X.; Tian, H.; Zhu, W.-H. Porphyrin Cosensitization for a Photovoltaic Efficiency of 11.5%: A Record for Non-Ruthenium Solar Cells Based on Iodine Electrolyte. *J. Am. Chem. Soc.* **2015**, *137*, 14055–14058. [CrossRef] [PubMed]
8. Mathew, S.; Yella, A.; Gao, P.; Humphry-Baker, R.; Curchod, B.F.; Ashari-Astani, N.; Tavernelli, I.; Rothlisberger, U.; Nazeeruddin, M.K.; Grätzel, M. Dye-sensitized solar cells with 13% efficiency achieved through the molecular engineering of porphyrin sensitizers. *Nat. Chem.* **2014**, *6*, 242–247. [CrossRef] [PubMed]
9. Kakiage, K.; Aoyama, Y.; Yano, T.; Oya, K.; Fujisawa, J.-I.; Hanaya, M. Highly-efficient dye-sensitized solar cells with collaborative sensitization by silyl-anchor and carboxy-anchor dyes. *Chem. Commun.* **2015**, *51*, 15894–15897. [CrossRef] [PubMed]
10. Kakiage, K.; Aoyama, Y.; Yano, T.; Oya, K.; Kyomen, T.; Hanaya, M. Fabrication of a high-performance dye-sensitized solar cell with 12.8% conversion efficiency using organic silyl-anchor dyes. *Chem. Commun.* **2015**, *51*, 6315–6317. [CrossRef] [PubMed]
11. Housecroft, C.E.; Constable, C.E. The Emergence of copper(I)-based dye sensitized solar cells. *Chem. Soc. Rev.* **2015**, *44*, 8386–8398. [CrossRef] [PubMed]
12. Magni, M.; Biagini, P.; Colombo, A.; Dragonetti, C.; Roberto, D.; Valore, A. Versatile copper complexes as a convenient springboard for both dyes and redox mediators in dyes sensiatized solar cells. *Coord. Chem. Rev.* **2016**, *322*, 69–93. [CrossRef]
13. Sandroni, M.; Pellegron, Y.; Odobel, F. Heteroleptic bis-diimine copper(I) complexes for applications in solar energy conversion. *Compt. Rendus Chim.* **2016**, *19*, 79–93. [CrossRef]
14. Jakubikova, E.; Bowman, D.N. Fe(II)-Polypyridines as Chromophores in Dye-Sensitized Solar Cells: A Computational Perspective. *Acc. Chem. Res.* **2015**, *48*, 1441–1449. [CrossRef] [PubMed]
15. Liu, Y.; Persson, P.; Sundström, V.; Wärnmark, K. Fe *N*-Heterocyclic Carbene Complexes as Promising Photosensitizers. *Acc. Chem. Res.* **2016**, *49*, 1477–1485. [CrossRef] [PubMed]
16. Malzner, F.J.; Brauchli, S.Y.; Constable, E.C.; Housecroft, C.E.; Neuburger, M. Halos show the path to perfection: peripheral iodo-substituents improve the efficiencies of bis(diimine)copper(I) dyes in dye-sensitized solar cells. *RSC Adv.* **2014**, *4*, 48712–48723. [CrossRef]
17. Sandroni, M.; Favereau, L.; Planchat, A.; Akdas-Kilig, H.; Szuwarski, N.; Pellegrin, Y.; Blart, E.; Le Bozec, H.; Boujtita, M.; Odobel, F. Heteroleptic copper(I)–polypyridine complexes as efficient sensitizers for dye sensitized solar cells. *J. Mater. Chem. A* **2014**, *2*, 9944–9947. [CrossRef]
18. Malzner, F.J.; Willgert, M.; Constable, E.C.; Housecroft, C.E. The way to panchromatic copper(I)-based dye-sensitized solar cells: Co-sensitization with the organic dye SQ2. *J. Mater. Chem. A* **2017**, *5*, 13717–13729. [CrossRef]
19. Fürer, S.O.; Bozic-Weber, B.; Schefer, T.; Wobill, C.; Constable, E.C.; Housecroft, C.E.; Willgert, M. Understanding why replacing I_3^-/I^- by cobalt(II)/(III) electrolytes in bis(diimine)copper(I)-based dye-sensitized solar cells improves performance. *J. Mater. Chem. A* **2016**, *4*, 12995–13004. [CrossRef]
20. Ashbrook, L.N.; Elliott, C.M. Dye-Sensitized Solar Cell Studies of a Donor-Appended Bis(2,9-dimethyl-1,10-phenanthroline) Cu(I) Dye Paired with a Cobalt-Based Mediator. *J. Phys. Chem. C* **2013**, *117*, 3853–3864. [CrossRef]
21. Fürer, S.O.; Luu, L.Y.N.; Bozic-Weber, B.; Constable, E.C.; Housecroft, C.E. Improving performance of copper(I)-based dye sensitized solar cells through I_3^-/I^- electrolyte manipulation. *Dyes Pigment.* **2016**, *132*, 72–78. [CrossRef]
22. Dragonetti, C.; Magni, M.; Colombo, A.; Melchiorre, F.; Biagini, P.; Roberto, D. Coupling of a Copper Dyes with a Copper Electrolyte: A Fascinating Springboard for Sustainable Dye-Sensitized Solar Cells. *ACS Appl. Energy Mater.* **2018**, *1*, 751–756. [CrossRef]
23. Büttner, A.; Brauchli, S.Y.; Vogt, R.; Constable, E.C.; Housecroft, C.E. Combining phosphonic acid-functionalized anchoring ligands with asymmetric ancillary ligands in bis(diimine)copper(I) dyes for dye-sensitized solar cells. *RSC Adv.* **2016**, *6*, 5205–5213. [CrossRef]
24. Brauchli, S.Y.; Malzner, F.J.; Constable, E.C.; Housecroft, C.E. Copper(I)-based dye-sensitized solar cells with sterically demanding anchoring ligands: Bigger is not always better. *RSC Adv.* **2015**, *5*, 48516–48525. [CrossRef]
25. Zhang, L.; Cole, J.M. Anchoring Groups for Dye-sensitized Solar Cells. *ACS Appl. Mater. Interfaces* **2015**, *7*, 3427–3455. [CrossRef] [PubMed]

26. Vioux, A.; Le Bideau, J.; Mutin, P.H.; Leclercq, D. Hybrid Organic–Inorganic Materials Based on organophosphorus Derivatives. *Top. Curr. Chem.* **2004**, *232*, 145–174. [CrossRef]
27. Wang, P.; Klein, C.; Moser, J.-E.; Humphry-Baker, R.; Cevey-Ha, N.-L.; Charvet, R.; Comte, P.; Zakeeruddin, S.M.; Grätzel, M. Amphiphilic Ruthenium Sensitizer with 4,4′-Diphosphonic Acid-2,2′-bipyridine as Anchoring Ligand for Nanocrystalline Dye Sensitized Solar Cells. *J. Phys. Chem. B* **2004**, *108*, 17553–17559. [CrossRef]
28. Bozic-Weber, B.; Brauchli, S.Y.; Constable, E.C.; Fürer, S.O.; Housecroft, C.E.; Wright, I.A. Hole-transport functionalized copper(I) dye sensitized solar cells. *Phys. Chem. Chem. Phys.* **2013**, *15*, 4500–4504. [CrossRef] [PubMed]
29. Malzner, F.J.; Prescimone, A.; Constable, E.C.; Housecroft, C.E.; Willgert, M. Exploring simple ancillary ligands in copper-based dye-sensitized solar cells: Effects of a heteroatom switch and of co-sensitization. *J. Mater. Chem. A* **2017**, *5*, 4671–4685. [CrossRef]
30. Schumacher, E.F. *Small Is Beautiful: A Study of Economics as if People Mattered*; Blond & Briggs Ltd.: London, UK, 1973.
31. Eggleston, M.K.; McMillin, D.R.; Koenig, K.S.; Pallenberg, A.J. Steric Effects in the Ground and Excited States of $Cu(NN)_2^+$ Systems. *Inorg. Chem.* **1997**, *36*, 172–176. [CrossRef]
32. Hammett, L.P. The Effect of Structure upon the Reactions of Organic Compounds. Benzene Derivatives. *J. Am. Chem. Soc.* **1937**, *59*, 96–103. [CrossRef]
33. McDaniel, D.H.; Brown, H.C. An Extended Table of Hammett Substituent Constants Based on the Ionization of Substituted Benzoic acids. *J. Org. Chem.* **1958**, *23*, 420–427. [CrossRef]
34. Hansch, C.; Leo, A.; Taft, R.W. A Survey of Hammett Substituent Constants and Resonance and Field Parameters. *Chem. Rev.* **1991**, *91*, 165–195. [CrossRef]
35. Wu, F.; Liu, J.; Wang, G.; Song, Q.; Zhu, L. *m*-Methoxy Substituents in a Tetraphenylethylene-Based Hole-Transport Material for Efficient Perovskite Solar Cells. *Chem. Eur. J.* **2016**, *22*, 16636–16641. [CrossRef] [PubMed]
36. Mukkala, V.M.; Kankare, J.J. New 2,2′-Bipyridine Derivatives and Their Luminescence Properties with Europium(III) and Terbium(III) Ions. *Helv. Chim. Acta* **1992**, *75*, 1578–1592. [CrossRef]
37. Constable, E.C.; Housecroft, C.E.; Neuburger, M.; Poleschak, I.; Zehnder, M. Functionalised 2,2′-bipyridine ligands for the preparation of metallostars; X-ray structures of free ligands and preparation of copper(I) and silver(I) complexes. *Polyhedron* **2003**, *22*, 93–108. [CrossRef]
38. Boudebous, A.; Constable, E.C.; Housecroft, C.E.; Neuburger, M.; Schaffner, S.; Listorti, A.; Sabatini, C.; Barigelletti, F. Preparation and photophysical studies of copper(I) and ruthenium(II) complexes of 4,4′-bis(3,5-dimethoxyphenyl)-6,6′-dimethyl-2,2′-bipyridine. *Inorg. Chim. Acta* **2009**, *362*, 1825–1830. [CrossRef]
39. Bozic-Weber, B.; Brauchli, S.Y.; Constable, E.C.; Fürer, S.O.; Housecroft, C.E.; Malzner, F.J.; Wright, I.A.; Zampese, J.A. Improving the photoresponse of copper(I) dyes in dye-sensitized solar cells by tuning ancillary and anchoring ligand modules. *Dalton Trans.* **2013**, *42*, 12293–12308. [CrossRef] [PubMed]
40. Kröhnke, F. The Specific Synthesis of Pyridines and Oligopyridines. *Synthesis* **1976**. [CrossRef]
41. Wenger, B.; Grätzel, M.; Moser, J.-E. Rationale for Kinetic Heterogeneity of Ultrafast Light-Induced Electron Transfer from Ru(II) Complex Sensitizers to Nanocrystalline TiO_2. *J. Am. Chem. Soc.* **2005**, *127*, 12150–12151. [CrossRef] [PubMed]
42. Thorsmølle, V.K.; Wenger, B.; Teuscher, J.; Bauer, C.; Moser, J.-E. Dynamics of Photoinduced Interfacial Electron Transfer and Charge Transport in Dye-Sensitized Mesoscopic Semiconductors. *CHIMIA Int. J. Chem.* **2007**, *61*, 631–634. [CrossRef]
43. Bozic-Weber, B.; Chaurin, V.; Constable, E.C.; Housecroft, C.E.; Meuwly, M.; Neuburger, M.; Rudd, J.A.; Schönhofer, E.; Siegfried, L. Exploring copper(I)-based dye-sensitized solar cells: A complementary experimental and TD-DFT investigation. *Dalton Trans.* **2012**, *41*, 14157–14169. [CrossRef] [PubMed]
44. Kubas, G.J. Tetrakis(Acetonitrile)Copper(I) Hexafluorophosphate. *Inorg. Synth.* **1979**, *19*, 90–92. [CrossRef]

45. Brauchli, S.Y.; Bozic-Weber, B.; Constable, E.C.; Hostettler, N.; Housecroft, C.E.; Zampese, J.A. Factors controlling the photoresponse of copper(I) diimine dyes containing hole-transporting dendrons in dye-sensitized solar cells. *RSC Adv.* **2014**, *4*, 34801–34815. [CrossRef]
46. *Spartan'16*; Wavefunction Inc.: Irvine, CA, USA, 2017.